JOURNAL OF MATERIALS SCIENCE 24 (1989) 298–306

A predictive model for particulate-filled composite materials

Part 1 *Hard particles*

F. J. GUILD
Department of Materials, Queen Mary College, Mile End Road, London E1 4NS, UK
R. J. YOUNG
Polymer Science and Technology Group, Manchester Materials Science Centre, University of Manchester Institute of Science and Technology, P.O. Box 88, Manchester M60 1QD, UK

A predictive model for particulate-filled composite materials has been developed. The model uses a combination of finite element analysis and spatial statistical techniques; this combination allows the results from finite element analysis to be applied to real materials. The model is applied to epoxy resin filled with glass spheres. Predicted values of stiffness are compared with experimental measurements, and excellent agreement is found. The model is used to investigate stress distributions and the results are compared with experimental observations of fracture under varying conditions; the fracture behaviour of these materials is significantly elucidated.

1. Introduction

Advancing technology is allowing the development of an increasing range of particulate-reinforced polymers. This development can be properly exploited only if it is matched with increasing understanding of the mechanical behaviour of these materials. A predictive model is required which allows the description of the properties of the composite material from the properties of the constituent materials.

Finite element analysis allows the development of such a predictive model. We use finite element analysis in conjunction with a specially developed statistical model of particulate reinforced materials, which is described in detail elsewhere [1]. Results from our finite element analysis can thus be related to real materials. This paper presents results for epoxy resin containing hard, glass, particles. Results for soft, rubber, particles are presented in Part 2 [2]. The theoretical predictions shed considerable light on the widely reported experimental results from these materials. Predictive results for a range of constituent material properties will be presented in a future paper [3].

Several authors have applied finite element analysis to composite materials. The problem of relating results from finite element analysis to the behaviour of real materials has been discussed by Adams [4]. Most applications, however, have been carried out at the macroscopic level, assuming homogeneous properties within a single layer of laminate. These applications include investigation of edge effects in laminated plates [5, 6], investigation of the effect of a hole [7], prediction of stress intensity factors [8] and calculation of thermal stresses [9]. Application of finite element analysis to the microscopic level of composite materials has previously necessitated gross assumptions regarding the arrangement of the fibres [10–13] or spheres [14, 15]. Recently Termonia [16] has used finite differences to predict stiffness of short-fibre and particulate-filled polymers; good agreement between predictions and experimental data was found. However, the material was modelled as simple cubic packing of the filler. Our combination of spatial statistical techniques and finite element analysis takes account of real filler distributions, and allows logical application of the results of finite elment analysis to real composite materials.

The failure of glass-filled epoxy resin has been extensively examined by several authors including Mallick and Broutman [17] and Spanoudakis and Young [18, 19]. Our theoretical predictions here may be compared with their experimental results. Stress distributions around a glass sphere in various polymer matrices have been experimentally examined, and predicted using finite element analysis, by Dekkers and Heikens [20–24]; their results are for very low volume fractions or single spheres. We can compare our theoretical predictions with their model.

2. Analysis

2.1. Finite element model

The development of the finite element model is shown in Fig. 1. Spherical particles of equal diameter are assumed to be randomly distributed within an infinite matrix. Finite element analysis is performed for a cylinder of resin, radius equal to half-height, R, containing a single sphere at its centre, radius r. This cylinder can be represented by the plane ABCD shown

0022–2461/89 $03.00 + .12

in Fig. 1 using axisymmetric elements, the y-axis being the axis of symmetry. Finite element analysis is carried out for a 1 radian segment. The imposed conditions of deflection are shown in Fig. 1b. The sides AB and AD remain stationary because these are lines of symmetry in the cylinder. The lines BC and CD remain parallel to their original directions arising from the equal and opposite forces of neighbouring material.

A typical finite element grid is shown in Fig. 1c. The elements used are eight-node quadrilateral axisymmetric elements, except at the centre of the sphere, A, where six-node triangular elements are used. The value of the sphere radius, r, was kept constant at 75 units; the value of the cylinder radius, R, was varied between 85 and 170 units. Grids for all values of R are similar to that shown in Fig. 1c, with fewer elements for smaller values of R. The grids were carefully derived from coarser grids and checked for validity by continuity of stress, especially around the interface, as described below, and by the absence of shear stress around the outside of the grid.

2.2. Finite element calculations

The finite element analysis package used is LUSAS, running on an ICL 2988 computer. Analysis was carried out for grids with various values of radius ratio, R/r. Linear elastic properties for epoxy resin and glass or rubber spheres were used. The shape of the deformed grid, shown in Fig. 1b, was achieved by loading the grid by prescribed displacement in the y-direction of the nodes along CD. Constraint equations were used for the nodes along BC constraining the x-displacements to be equal.

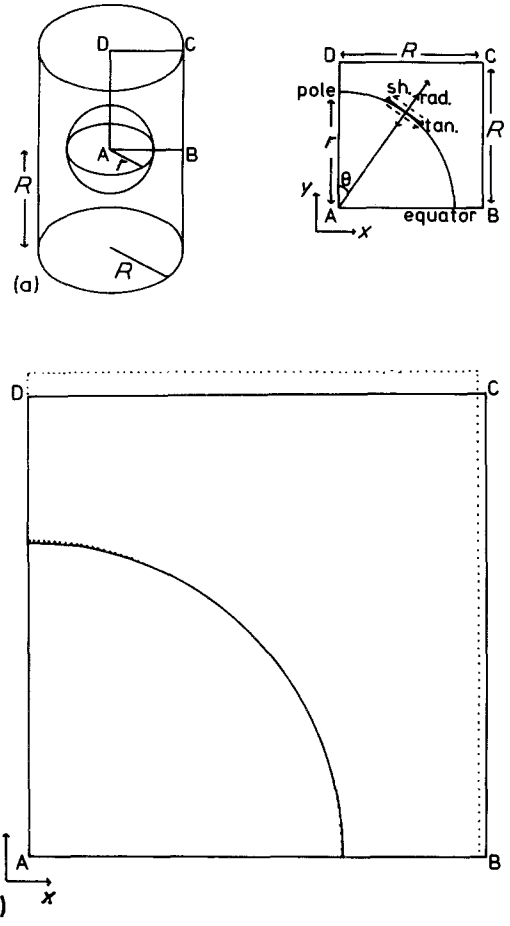

Results from LUSAS include stresses in three dimensions and the reactions to earth for nodes around the outside of the grid. Post-processing of results was added to transform the stresses around the interface to polar coordinates. The average stress applied to the material is calculated from the sum of the reactions to earth for the nodes along CD, for the 1 radian segment. All stress results are presented as stress concentration factors, the ratio of that stress to the average applied stress. The Youngs modulus, E, is calculated from the applied strain and the average applied stress. Further stress results output by LUSAS include principal stresses and Von Mises stress. The Von Mises stress, σ_V, is defined by

$$\sigma_V = (1/2\,(\sigma_x - \sigma_y)^2 + 1/2\,(\sigma_y - \sigma_z)^2 + 1/2\,(\sigma_z - \sigma_x)^2 + 3\sigma_{xy}^2)^{1/2}$$

where the axes x, y, z are defined in Fig. 1.

The yield of polymers is best described by the modified Von Mises yield criterion [25]; yield occurs when the von Mises stress, defined above, reaches a critical value, the magnitude of that critical value being additionally dependent on the hydrostatic stress. Hydrostatic stresses are easily calculated from the principal stresses in the LUSAS output.

2.3. Statistical Model

The statistical model has been described in detail elsewhere [1]. The model is based on the calculation of the distribution of the distance from a sphere centre to the boundary of its Voronoi cell; the Voronoi cell is the volume around a sphere closer to that sphere than any other sphere. The spheres are assumed to be randomly distributed, but the spheres are not allowed to overlap; that is, they are distributed as a Gibbs hard-core process.

Results from a single finite element grid cannot be directly related to a volume fraction of spheres. Analysis must be carried out for the primary grid, whose

Figure 1 Development of the finite element model. (a) Representation of sphere in a cylinder using axisymmetric elements. (b) Comparison of (——) original and (. . .) deformed grids. (c) Typical finite element grid.

TABLE I Constituent material properties

Resin matrix		Glass sphere		Reference
Young's modulus (GPa)	Poisson's ratio	Young's modulus (GPa)	Poisson's ratio	
3.01	0.394	76.0	0.23	[26]
3.208	0.35	73.1	0.21	[27]

dimensions are directly related to the required volume fraction, and two additional grids for calculation of the dispersion factors. These factors must be applied for exact results to take into account that in real material the interparticle distances are variable. Further, the model of the material as consisting of cylinders of varying size gives rise to two different predicted values for a property. The cylinders contribute differently to the overall property of the material for different properties, and according to the assumption made regarding the distribution of load to the cylinders. We have implemented two bounds, namely that the cylinders are at equal stress or equal strain. We find these bounds to be very close, and our theoretical predictions are presented as these bounds.

2.4. Implementation

The implementation has been fully described elsewhere [1]. Finite element analysis was carried out for grids with cylinder radius, R, varying between 85 and 170 units; the sphere radius was constant at 75 units. Additional grids were analysed to allow the calculation of the dispersion factors. Volume fractions of spheres analysed thus varied between 5.72% and 49.19%, around the limit of the theoretical analysis [1]. The material properties used are shown in Table I.

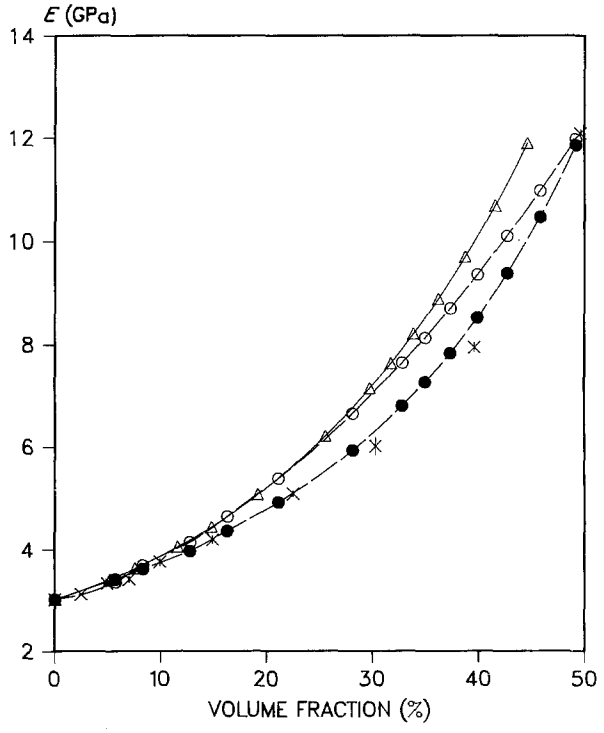

Figure 2 Variation of Young's modulus, E, with volume fraction for epoxy resin filled with glass spheres. (●) Equal stress, (○) equal strain, predicted values using our model. (△) Predicted values assuming regular hexagonal array; (x) experimental values, with error bars [26].

The results from LUSAS were manipulated for the calculation of overall Young's modulus, E; these predictions are directly comparable with experimental results. Stress systems were examined using contour diagrams produced by the LUSAS graphics package, MYSTRO. These diagrams are most illuminating, but it must be emphasized that the numerical results shown by them are inaccurate because dispersion factors have not been applied; the contour diagrams do not show the correct results because the statistical variability of the interparticle distance has not been taken into account. Precise values of stress concentration factor at the points of interest indicated by the contour diagrams were calculated and are presented graphically as functions of volume fraction. These values of stress concentration factor have been calculated using our model, with the application of dispersion factors which take into account the effect of the statistical variability of the interparticle distance. These predictions may be compared with experimental results describing yield and fracture of these materials.

3. Young's modulus

Careful measurements of values of Young's modulus of epoxy resin reinforced with glass spheres are available in the literature [26]. Finite element analysis was carried out for constituent material properties in that reference (Table I). Predicted values of Young's modulus are compared with those experimental values in Fig. 2. Agreement is excellent throughout the range of volume fraction. Fig. 2 also includes predicted results assuming regular arrangement of spheres [15]. Agreement is far closer for our model, particularly at higher volume fractions. Further, our model does not include the inherent logical inconsistency of using axisymmetric elements for a regular arrangement [1].

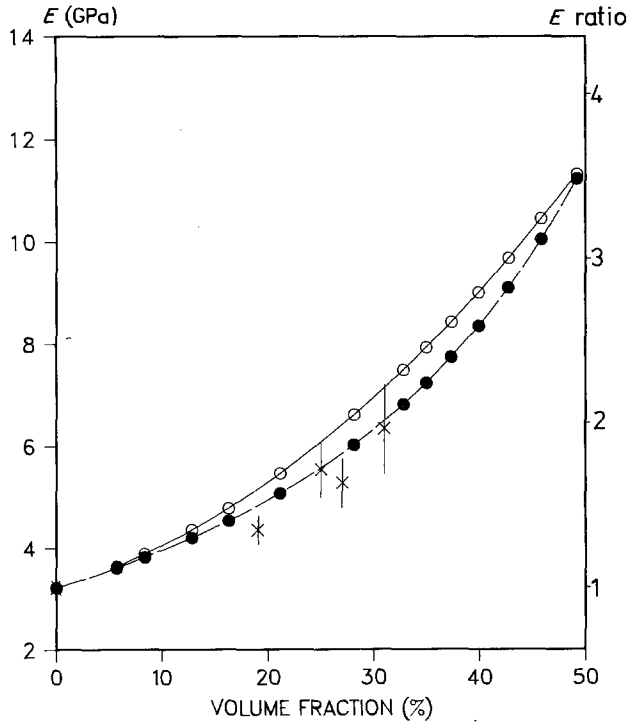

Figure 3 Variation of Young's modulus, E, with volume fraction for epoxy resin filled with glass spheres. (●) Equal stress, (○) equal strain, predicted values. (x) Experimental values, with error bars [27].

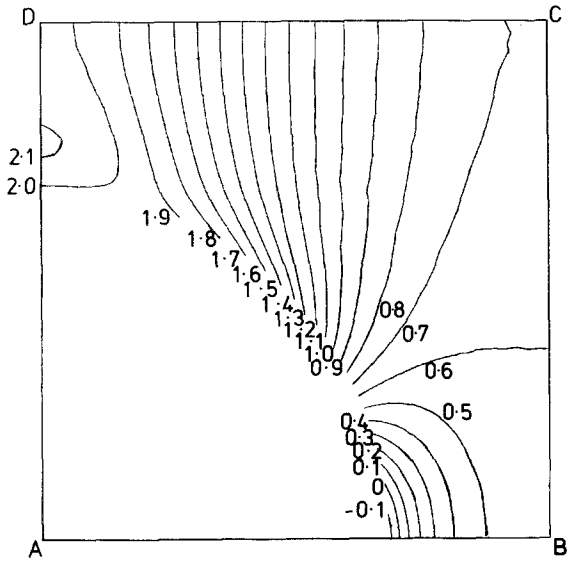

Figure 4 Contours of stress concentration factor of applied stress, σ_{yy}, for primary grid for epoxy resin filled with 21.1% volume fraction of glass spheres.

This excellent agreement allows confident further predictions to be made using our model.

Further comparison between our predictions and experimental values of Young's modulus is presented in Fig. 3. The experimental values are from Maxwell [27], obtained at various temperatures, that is for various values of matrix modulus. The Young's modulus plotted is therefore the ratio of the composite to matrix moduli, averaged for twelve different temperatures; values varying from the mean by more than two standard deviations were discarded. The error bars denote one standard deviation. Reasonable agreement is found throughout the range of volume fraction.

4. Stress distribution

4.1. Concentration of direct stress

Stress distributions are examined using constituent material properties measured by Maxwell [27], shown in Table I. The applied stress is a direct σ_{yy} stress; a contour diagram for the concentration of this stress in the resin is shown in Fig. 4. This contour diagram is for the primary grid corresponding to 21.1% volume fraction occupied by spheres.

Maximum stress concentration is found in the resin just above the pole of the sphere. Examination of other contour diagrams confirmed that this is the maximum principal stress. This position is in agreement with previous theoretical results and experimental observations [19]. The precise position and value of this maximum stress concentration factor varies with volume fraction, as shown in Fig. 5. The magnitude of the stress concentration of applied stress increases with increasing volume fraction of glass. This result is not surprising and may be described as arising from increasing interaction between the stress fields around particles as their separation decreases.

The position of maximum stress concentration factor of applied stress varies as shown in Fig. 5. At high volume fractions its position is at the edge of the grid, that is midway between particles. At lower volume fractions the position is relatively closer to the particle in the cylinder under analysis, that is further away from the adjacent particle. Taking into account the varied distances between adjacent particles for different volume fractions, that maximum distance between the position of stress concentration and the adjacent particle was calculated. This distance decreases rapidly with increasing volume fraction; expressed in terms of the sphere radius its value is decreased from 243% at the lowest volume fraction

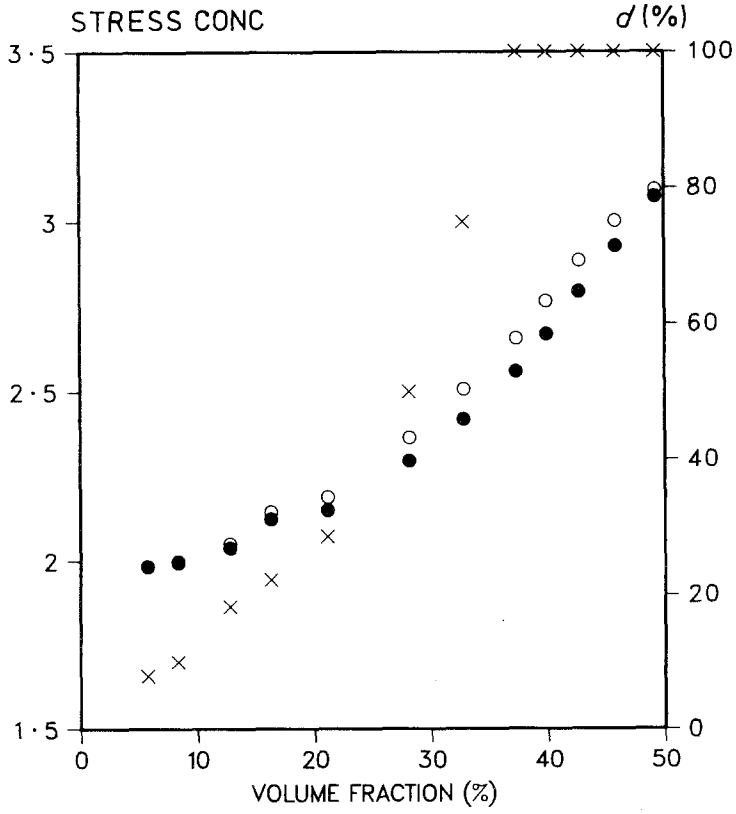

Figure 5 Variation of stress concentration factor of applied stress, σ_{yy}, with volume fraction, and relative distance, d, between sphere pole and edge of grid, for epoxy resin filled with glass spheres. (●) Equal stress, (○) equal strain, stress concentration factor. (x) Position d.

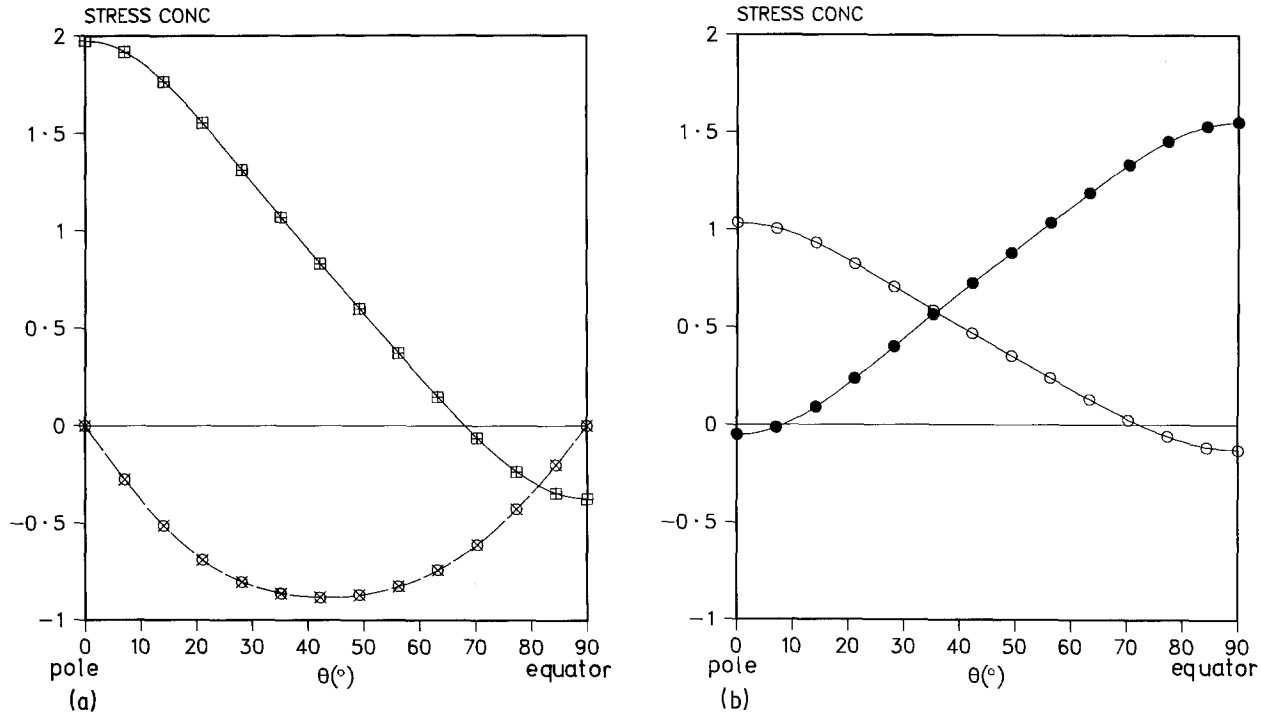

Figure 6 Variation of stress concentration factors of interface stresses, in polar coordinates, for primary grid for epoxy resin filled with 21.1% glass spheres. (a) Radial and shear stresses: (□) radial stress in resin; (○) shear stress in resin; (+) radial stress in glass; (x) shear stress in glass. (b) Tangential stresses: (○) tangential stress in resin; (●) tangential stress in glass.

analysed (5.72%), to 9.3% at the highest volume fraction analysed (49.2%).

4.2. Stresses at the interface

Stresses around the interface were transformed to polar coordinates using the notation shown in Fig. 1. Results for the same primary grid, volume fraction 21.1%, are shown in Fig. 6. Radial and shear stresses on either side of the interface, in the glass and resin, are identical, as required. Tangential stresses in the two materials are not identical, and are not required to be identical. The excellent agreement in radial and shear stresses around the interface is a stringent test for the validity of the finite element grid. Substantial stress is transferred to the glass sphere (Fig. 6). This leads to the sharp increase in stiffness with volume fraction (Fig. 2), which has been found to be in excellent agreement with experimental results.

Maximum radial stress is at the pole of the sphere where it is the σ_{yy} stress; variation of the value of this stress concentration factor with volume fraction is similar to that of the maximum stress concentration factor shown in Fig. 5. Radial stress is tensile at the pole of the sphere and compressive at the equator; the zero position, at $\theta = 68°$ is identical for all volume fractions. There is a maximum in radial–tangential shear stress at $\theta = 42.2°$ for this grid. Both the value and position of this stress concentration factor vary

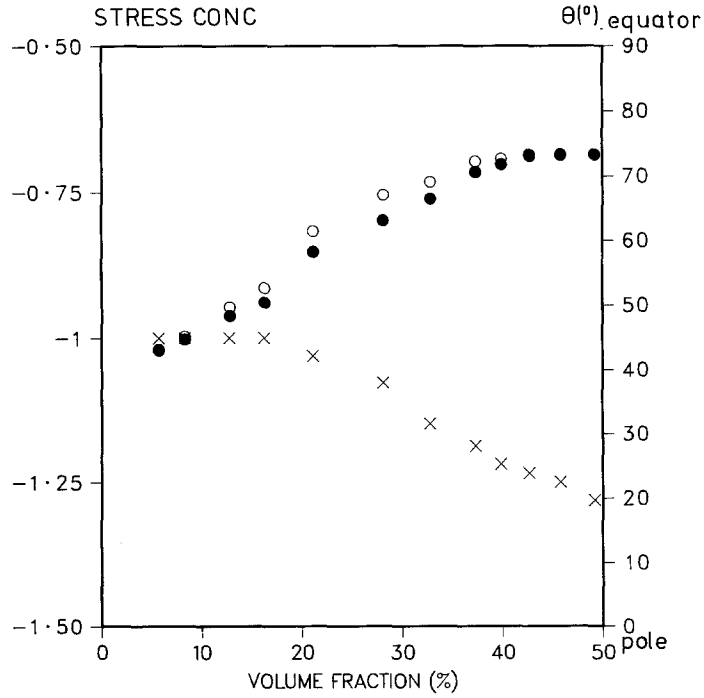

Figure 7 Variation of stress concentration factor of maximum shear stress at the interface, and position, θ, with volume fraction, for epoxy resin filled with glass spheres. (●) Equal stress, (○) equal strain, stress concentration factor. (x) Position θ.

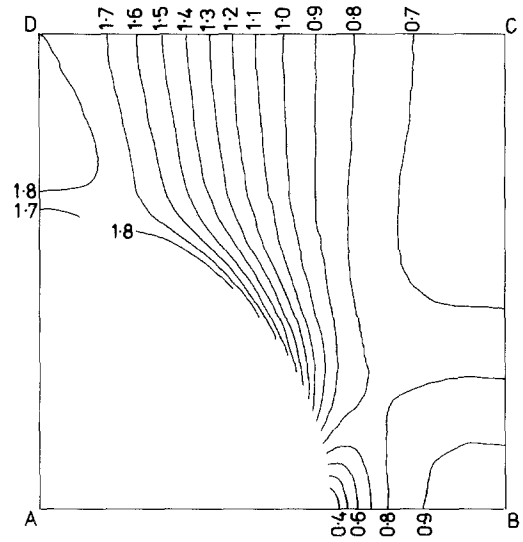

Figure 8 Contours of stress concentration factor of Von Mises stress, σ_V, for primary grid for epoxy resin filled with 16.3% volume fraction of glass spheres.

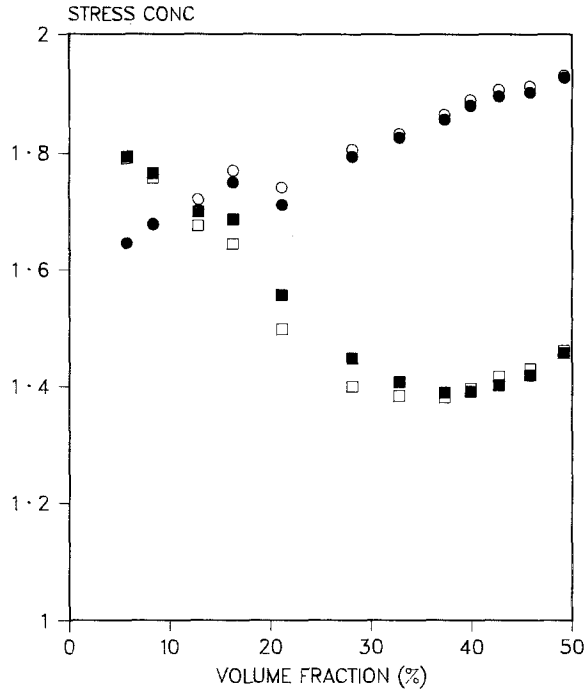

Figure 9 Variation of stress concentration factors of Von Mises stress with volume fraction for epoxy resin filled with glass spheres. (●) Equal stress, (○) equal strain, stress concentration above pole. (■) Equal stress, (□) equal strain, stress concentration at interface.

with volume fraction, as shown in Fig. 7. The absolute value of this stress concentration factor decreases with increasing volume fraction. This decrease is explained by description of the source of this stress concentration, namely the difference in moduli between the particle and its surrounding material. As the volume fraction of spheres increases this difference decreases, so the magnitude of the stress concentration decreases. We note, however, that the magnitude of this decrease is far smaller than the magnitude of the increase for the concentration of applied stress, by about a factor of four. At high volume fractions the site of this maximum concentration of shear stress moves closer to the pole of the sphere.

Stresses around the interface of spherical particles have previously been considered for a single hard particle [23]. For a poorly bonded interface they postulate that a crack will form around the interface for tensile radial stress. Using finite element analysis, for a glass sphere in epoxy resin, using constituent material properties very close to those used here, they predicted that the interfacial crack should grow to an angle $\theta = 68$ to 70° depending on the friction remaining in the debonded interface. The experimental value was measured to be about 60°. These results are in agreement with our predicted value of $\theta = 68°$, constant for all volume fractions.

Tensile radial stress at the interface causes debonding, as observed by Dekkers and Heikens [23]. The magnitude of the stress concentration of radial stress at the pole is not much smaller than the maximum stress concentration of applied stress (Figs 5 and 6), so, for tensile loading, debonding from the pole would be expected. We note that for applied tensile stress the radial stress at the equator is compressive (Fig. 6). This stress would be tensile if the applied stress was compression; although the absolute magnitude of this stress concentration factor is around an order of magnitude smaller than at the pole it could be sufficient to cause debonding from the equator of the sphere under conditions of applied compression.

4.3. Concentration of yield stress

The Von Mises stress, as defined in Section 2.2 above, is calculated by LUSAS and can be output as a counter diagram; an example, for the primary grid corresponding to 16.3% volume fraction, is shown in Fig. 8. Two positions of maximum von Mises stress are found; the first in the resin above the pole of the sphere, near but not precisely at the same position as the maximum direct stress concentration (Fig. 4); the second at the interface at $\theta = 42°$, near but not precisely at the same position as the maximum shear stress at the interface (Fig. 7). The values of these stress concentration factors vary with volume fraction, as shown in Fig. 9. Their positions vary in the same directions as the positions of the associated concentrations of direct stresses (Figs 5 and 7). Fig. 9 shows that the magnitudes of the two concentrations of Von Mises stress vary with volume fraction in the same way as the associated stress concentrations, although the range of variation is very small. The maximum above the pole is greater at high volume fractions, but at low volume fractions, below around 12%, the maximum at the interface is greater. There is a discontinuity in the curve where the position of maximum Von Mises stress above the pole moves nearer to the particle from the edge of the grid, between volume fractions 16.28% and 21.13%.

Dekkers and Heikens [24] observed shear band formation for very low volume fractions of glass beads in various polymer matrices. They found shear band formation at the interface, at $\theta = 45°$. Our results (Fig. 9) show that at low volume fractions the maximum concentration of Von Mises stress is at the interface, at $\theta = 42°$. Our model is in agreement with their experimental observations.

The Von Mises stress at which yield occurs is dependent on the hydrostatic stress [25]. The hydrostatic

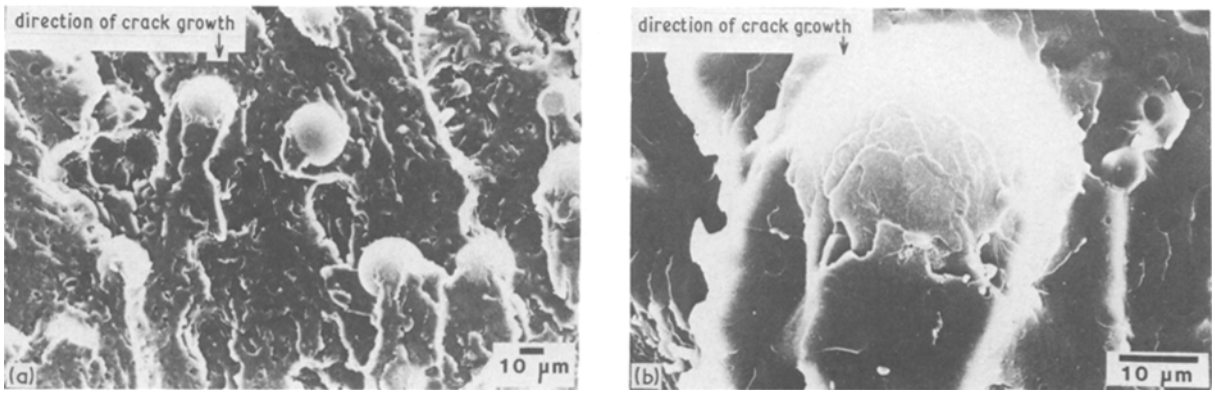

Figure 10 Fracture surface of a rubber-toughened epoxy resin filled with well-bonded glass spheres showing crack growth around the pole and resin smearing. The specimen was fractured at −70° C (from Maxwell [27]). (a) Low magnification, (b) high magnification.

stresses at the points of maximum Von Mises stress were calculated. For the application of tensile stress the hydrostatic stress was tensile. The stress concentration at the site above the pole varied between about 0.8 and 1.8 over the range of volume fraction. The hydrostatic stress concentration at the interface site is about 0.2 less than that at above the pole throughout the range of volume fraction. Both values remain almost constant up to around 20% volume fraction, but increase rapidly at higher volume fractions. The maximum concentration of hydrostatic stress in the matrix is at the pole of the sphere.

The variation of compressive yield strength with volume fraction was investigated by Mallick and Broutman [17]. They found that the compressive yield strength increases with increasing volume fraction of glass; the magnitude of this increase is hard to assess from their reported results, but the yield strength at 19% volume fraction of glass spheres appears about twice that of unfilled resin. The value appears unchanged between volume fractions 19% and 28%, but then increases again for 36%. The yield point is less distinct at high volume fractions. We believe this behaviour can be explained by examination of our predictions in Fig. 9. The tests were carried out in compression, so the hydrostatic stress concentration would increase the stress required for yield to occur. Fig. 9 shows that at high volume fractions yield would occur above the pole. There is a slight increase in the stress concentration with increasing volume fraction, but a large increase in the hydrostatic stress concentration; yield would therefore occur at higher applied stress with increasing volume fraction, as found. At lower volume fractions hydrostatic stress hardly changes with volume fraction. Fig. 9 shows that yield would occur at the interface, and the value of this stress concentration factor decreases with increasing volume fraction; yield would therefore also occur at higher applied stress with increasing volume fraction, as found. We postulate that the intermediate region, where the compressive yield strength appears constant with increasing volume fraction, corresponds to the crossover point for the yield positions shown in Fig. 9, noting that this crossover would be expected at a higher volume fraction than shown in Fig. 10 because the hydrostatic stress above the pole is always greater than that at the interface.

5. Fracture behaviour

The fracture of epoxy resin reinforced with glass spheres under various conditions has been studied by Spanoudakis and Young [18, 19], and Maxwell [27]. Their observations of fracture behaviour may be correlated with results from our model.

Crack growth is generally considered to be attracted to the position of maximum direct stress. Our model predicts that the position of maximum direct stress is above the pole (Fig. 5). These predictions correlate with experimental observations, shown in Fig. 10. For a well-bonded sphere, at low volume fractions, crack growth is attracted to the resin above the pole of the sphere (Fig. 10a). Smearing of resin around the pole of the sphere is observed (Fig. 10b). This fracture appearance contrasts with that observed for crack growth in epoxy resin containing poorly bonded glass

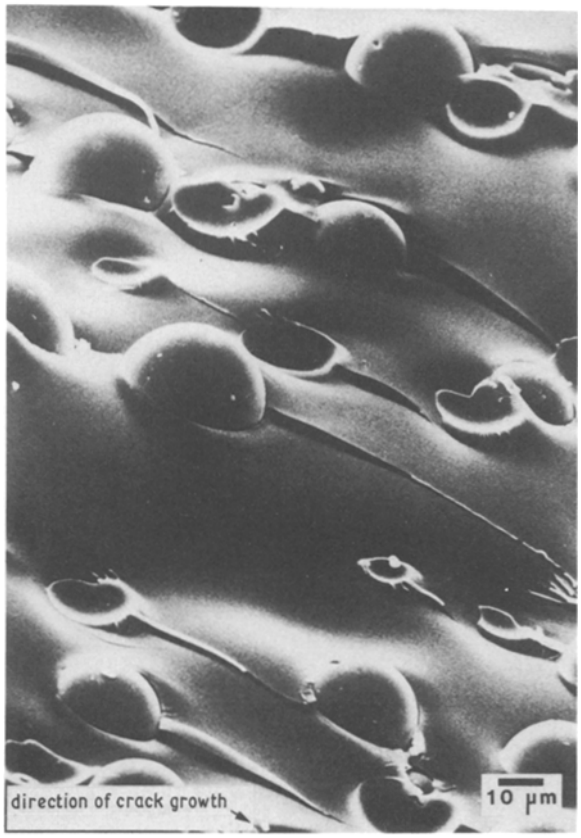

Figure 11 Fracture surface of epoxy resin filled with poorly bonded glass spheres showing crack growth towards the equator (from Maxwell [27]).

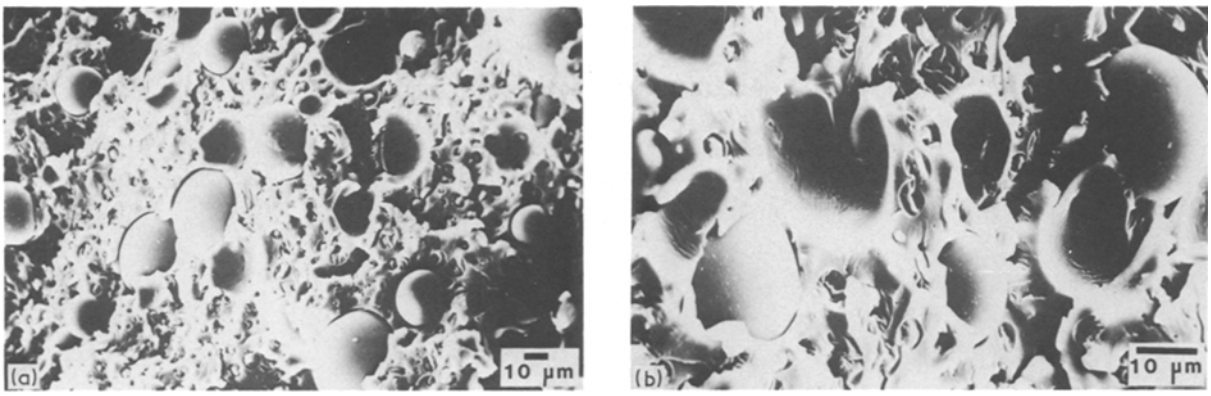

Figure 12 Fracture surface of a rubber-toughened epoxy resin filled with bonded glass spheres tested at high temperature showing domes of spheres. The specimen was fractured at 50° C (from Maxwell [27]). (a) Low magnification, (b) high magnification.

particles; crack growth is found to be attracted to the equator of the sphere (Fig. 11). The poorly bonded sphere must result in similar stress distribution in the resin to that for a hole, considered in Part 2 [2]; the site of maximum stress concentration is found to be at the equator of the sphere. Our predictions have been successfully used to describe the observed different fracture behaviour arising from the adhesion.

The amount of resin smearing around the pole of the well-bonded sphere would be dependent on the position of the crack with respect to the sphere. Our results (Section 4.1) have shown that at low volume fractions the maximum distance is much further away from a sphere than for high volume fractions. Thus our model predicts that more smearing would occur at low volume fractions, when crack growth could occur with no spheres visible in the fracture surface. Greater smearing at low volume fractions has been observed [18].

Change in fracture appearance has also been observed with change in constituent material properties for well-bonded glass spheres [27]. The usual fracture appearance for well-bonded spheres has been shown in Fig. 10; crack growth is attracted above the pole [19]. This appearance contrasts with that found for tests at high temperature, shown in Fig. 12; this test was carried out at 50° C, resulting in a decrease in resin stiffness of around 35%. The crack appears to have grown towards the interface, leaving a dome of sphere visible on the fracture surface.

We note that this dome of sphere visible in the fracture surface seems to imply that crack growth has been attracted to the position of maximum concentration of Von Mises stress at the interface, which varies in position from $\theta = 42°$ at low values of volume fraction to $\theta = 14°$ at high values of volume fraction. The magnitude of this stress concentration factor is dependent on the difference between the sphere properties and the properties of the surrounding material, and would thus increase for softened resin at increased temperature. We postulate that the change in fracture appearance with increasing temperature may imply that crack growth is attracted to the position of maximum Von Mises stress, which is predicted by our model to change position from above the pole to the interface with increasing temperature. Further experimental work is required to investigate this hypothesis. The mechanism of crack growth may be further elucidated by future improvement of the finite element model incorporating non-linear material properties.

6. Concluding remarks

Our predictive model for particulate-filled composite materials containing hard particles has produced interesting and useful results. The finite element model has been validated by the excellent agreement in values of stiffness between our predictions and careful experimental measurements. The predicted stress distributions are validated by the exact matching of stresses around the interface. Predicted stress distributions for epoxy resin filled with glass spheres have been successfully correlated with previous models and experimental observations. The successful description of the fracture appearance of these materials under various conditions leads to better understanding of their fracture behaviour, which will allow more confident use of these materials under different conditions.

Acknowledgements

We thank Dr P. J. Davy, Dr W. R. Davies and Dr J. W. Wright for valuable discussions. We acknowledge the interest and help in running LUSAS from F.E.A. Ltd and staff of the computer centre at Queen Mary College. F. J. Guild is now also an honorary research fellow in the Department of Mechanical Engineering, Plymouth Polytechnic, UK.

References

1. P. J. DAVY and F. J. GUILD, *Proc. Roy. Soc. Ser. A* **418** (1988) 95.
2. F. J. GUILD and R. J. YOUNG, *J. Mater. Sci.* in press.
3. *Idem*, in preparation.
4. D. F. ADAMS, *Fibre Sci. Technol.* **7** (1974) 111.
5. J. D. WHITCOMB, I. S. RAJU and J. G. GOREE, *Computers and Structures* **15** (1982) 23.
6. H. V. LAKSHMINARAYANA, *J. Compos. Mater.* **17** (1983) 357.
7. L. CARLSSON, *ibid.* **17** (1983) 238.
8. H. V. LAKSHMINARAYANA, *ibid.* **17** (1983) 227.
9. O. H. GRIFFIN and J. C. ROBERTS, *ibid.* **17** (1983) 539.
10. A. S. CARRARA and F. J. McGARRY, *ibid.* **2** (1968) 222.
11. M. J. IRONMONGER and W. G. WOOD, *J. Strain Anal.* **4** (1969) 121.
12. *Idem, ibid.* **5** (1970) 180.
13. W. L. KO, *J. Compos. Mater.* **12** (1978) 97.

14. B. D. AGARWAL, G. A. PANIZZA and L. J. BROUTMAN, *J. Amer. Ceram. Soc.* **54** (1971) 620.
15. B. D. AGARWAL and L. J. BROUTMAN, *Fibre Sci. Technol.* **7** (1974) 63.
16. Y. TERMONIA, *J. Mater. Sci.* **22** (1987) 1733.
17. P. K. MALLICK and L. J. BROUTMAN, *Mater. Sci. Engng* **18** (1975) 63.
18. J. SPANOUDAKIS and R. J. YOUNG, *J. Mater. Sci.* **19** (1984) 473.
19. *Idem, ibid.* **19** (1984) 487.
20. M. E. J. DEKKERS and D. HEIKENS, *ibid.* **18** (1983) 3281.
21. *Idem, J. Mater. Sci. Lett.* **3** (1984) 307.
22. *Idem, J. Mater. Sci.* **19** (1984) 3271.
23. *Idem, ibid.* **20** (1985) 3865.
24. *Idem, ibid.* **20** (1985) 3873.
25. P. B. BOWDEN, "The Yield Behaviour of Glassy Polymers", in "The Physics of Glassy Polymers", edited by R. N. Haward (Applied Science, London, 1973) Ch. 5.
26. J. C. SMITH, *J. Res. Nat. Bur. Stand. (Phys. Chem.)* **80A** (1976) 1.
27. D. L. MAXWELL, PhD Thesis, University of London (1987).

Received 11 January
and accepted 9 May 1988